Magnetic Resonance Imaging of Cartilage in the Athlete: Current Techniques and Spectrum of Disease

By Michael K. Shindle, MD, Li F. Foo, FRCR, Bryan T. Kelly, MD, A. Jay Khanna, MD,
Benjamin G. Domb, MD, Adam Farber, MD, Tony Wanich, MD, and Hollis G. Potter, MD

Introduction

In the athletic population, reproducible imaging of cartilage damage is vital for treatment considerations. With appropriate pulse sequencing, magnetic resonance imaging has been shown to be an accurate noninvasive method for the evaluation of articular cartilage injuries and for evaluating postoperative changes following chondral repair. In addition, magnetic resonance imaging does not utilize ionizing radiation, has direct multiplanar capabilities, and allows high-resolution imaging of soft-tissue structures. The purposes of the present review are to update orthopaedic surgeons on the applications and techniques for magnetic resonance imaging of cartilage in the athletic population, to define the normal magnetic resonance imaging characteristics of articular cartilage, to illustrate the spectrum of articular cartilage lesions that are detectable with magnetic resonance imaging, and to review normal and abnormal magnetic resonance imaging findings following cartilage repair.

Educational Objectives

After reviewing this article, the reader should (1) have a basic understanding of pulse sequences and terminology for cartilage-sensitive magnetic resonance imaging, including proton-density-weighted high-resolution fast-spin-echo sequences; (2) be able to identify normal and abnormal articular cartilage in the hip, knee, elbow, shoulder, and ankle; and (3) be able to identify normal and abnormal findings on postoperative magnetic resonance images after chondral repair techniques.

Basic Science of Articular Cartilage

An understanding of the structure of articular cartilage is crucial in order to understand the magnetic resonance imaging appearance of normal and abnormal cartilage morphology and is also the basis for the development of new imaging techniques. Articular cartilage is a viscoelastic material composed of chondrocytes (approximately 1%) embedded in an organized extracellular matrix composed primarily of water (65% to 80%), collagen, and proteoglycan. The predominant collagen is type II (95%), although smaller amounts of other collagen types (types IV, VI, IX, X, and XI) have been identified[1]. Collagen provides the structural framework and tensile strength of articular cartilage. Chondroitin and keratin sulfates are the predominant types of proteoglycan molecules that are negatively charged and attract cations and water, which provides compressive strength to the cartilage.

The normal thickness of articular cartilage ranges from 2 to 5 mm and is determined by the contact pressures that occur across a joint. Higher peak pressures result in thicker cartilage, and the patellofemoral joint has the thickest articular cartilage in the body. Articular cartilage can be divided into four distinct zones. The superficial zone accounts for 10% to 20% of the thickness and has the highest collagen content. In this zone, the collagen fibers are highly organized
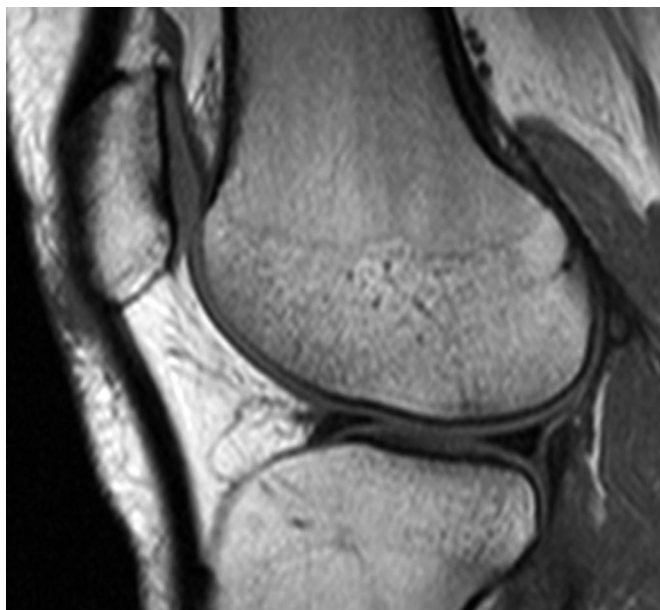

Fig. 1

Sagittal non-fat-suppressed T1-weighted spin-echo magnetic resonance image of the knee, demonstrating poor differential contrast between the intermediate signal intensity of cartilage and the low to intermediate signal intensity of joint fluid.
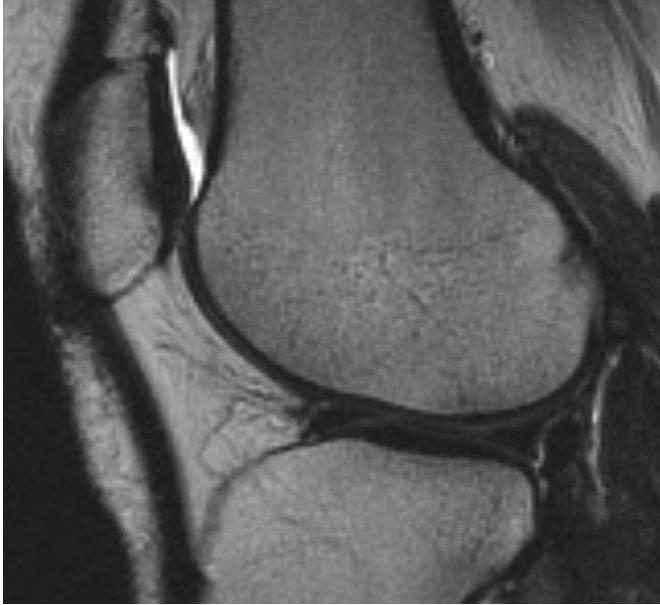
Fig. 2

Sagittal non-fat-suppressed T2-weighted spin-echo magnetic resonance image of the knee, demonstrating poor distinction between the deep components of cartilage and the adjacent subchondral plate.

Fig. 3

Sagittal three-dimensional fat-suppressed T1-weighted gradient-echo magnetic resonance image of the knee, demonstrating high contrast between hyperintense articular cartilage and hypointense bone.

and oriented parallel to the cartilage surface, which accounts for the high tensile strength. The transitional or middle zone accounts for 40% to 60% of the thickness and has a higher compressive modulus than the superficial zone. The collagen fibers are randomly oriented in this zone[2]. The radial zone has highly organized collagen fibers that are oriented parallel to the cartilage surface. In addition, this zone has the highest proteoglycan content and the lowest water content. The final zone is the calcified cartilage layer. The tidemark is a line that represents the boundary between uncalcified and calcified cartilage.

Cartilage-Insensitive Pulse Sequences

Many different pulse sequences have been described for the evaluation of articular cartilage. Traditional T1-weighted imaging provides poor differential contrast between the intermediate signal intensity of cartilage and the low to intermediate signal intensity of joint fluid (Fig. 1). In addition, this pulse sequence requires relatively long scan times. In conventional spin-echo T2 weighting, the long echo time results in poor delineation between the subchondral bone and the deep component of cartilage. This results in factitious thickening of the subchondral bone and thinning of the articular cartilage (Fig. 2).

Cartilage-Sensitive Pulse Sequences

T1-weighted three-dimensional fat-suppressed gradient-echo imaging demonstrates high contrast between the low signal intensity of bone and the high signal intensity of articular cartilage (Fig. 3). This makes it amenable to semi-automated cartilage segmentation algorithms for volume and

Fig. 4

Sagittal non-fat-suppressed intermediate echo-time fast-spin-echo magnetic resonance image of the knee, demonstrating the intermediate signal intensity of articular cartilage and gray-scale stratification, which corresponds to cartilage zonal anatomy.

thickness measurements. However, this sequence is less sensitive to partial-thickness cartilage defects, is not suitable for meniscal or ligamentous evaluation, undergoes degradation of

Fig. 5-A

Fig. 5-B

Figs. 5-A and 5-B Coronal fast-spin-echo magnetic resonance image (Fig. 5-A) and corresponding gradient-echo magnetic resonance image (Fig. 5-B) of the elbow in a patient with medial collateral ligament reconstruction, demonstrating susceptibility artifact in the presence of metallic suture anchor fixation (arrowheads).

the signal in the presence of metal, and requires a relatively long scan time[3].

Intermediate echo-time two-dimensional non-fat-suppressed fast/turbo spin-echo imaging provides good differential contrast between the intermediate signal intensity of articular cartilage, the low signal intensity of fibrocartilage, and the high signal intensity of synovial fluid (Fig. 4). This sequence also demonstrates gray-scale stratification, which corresponds to cartilage zonal anatomy. Thus, the signal corresponding to the deep zone of normal articular cartilage is hypointense because of the highly ordered collagen orientation and restriction of water mobility. Water is less restricted in the middle and superficial zones and thus has a relatively higher signal compared with the deep zone and subchondral bone. This subtly increasing signal is referred to as gray-scale stratification. With proper technique, this sequence has the ability to detect partial-thickness chondral lesions[4]. The other advantages of this sequence are that it is sensitive even in the presence of metal (Figs. 5-A and 5-B) and has very good differential contrast between the underlying bone, cartilage, ligaments, menisci, and joint fluid. A potential disadvantage is that a factitious loss of the subchondral plate and abnormal high signal in cartilage due to chemical shift misregistration

can occur at the subchondral bone-cartilage interfaces. This can be minimized by the use of a wider received bandwidth[3].

When fat suppression is applied to intermediate echo-time fast/turbo spin-echo imaging, the previously subtle differences between cartilage, fluid, and synovium become more readily discernable. In addition, as the contrast range is "rescaled," the detection of bone marrow and soft-tissue edema becomes possible (Fig. 6). This technique may provide an increased level of detail, but objective differences in accuracy have not been demonstrated[5]. In addition, the use of fat suppression typically requires lower in-plane resolution in order to maintain an adequate signal-to-noise ratio.

Many authors have advocated the use of magnetic resonance arthrography for the evaluation of articular cartilage because of its ability to accurately delineate intra-articular structures[6-8]. However, this converts magnetic resonance imaging into an invasive procedure and is associated with increased cost and imaging time.

Although the optimal pulse sequence is controversial, the Articular Cartilage Imaging committee, a subcommittee of the International Cartilage Repair Society (ICRS), recommends using fast-spin-echo imaging with proton density-weighted imaging with or without fat saturation, T2-weighted

Fig. 6
Sagittal fat-suppressed intermediate echo-time fast-spin-echo magnetic resonance image of the knee is fluid sensitive. The high signal intensity of the joint fluid and bone marrow edema pattern in the inferior pole of the patella are more easily discernable.
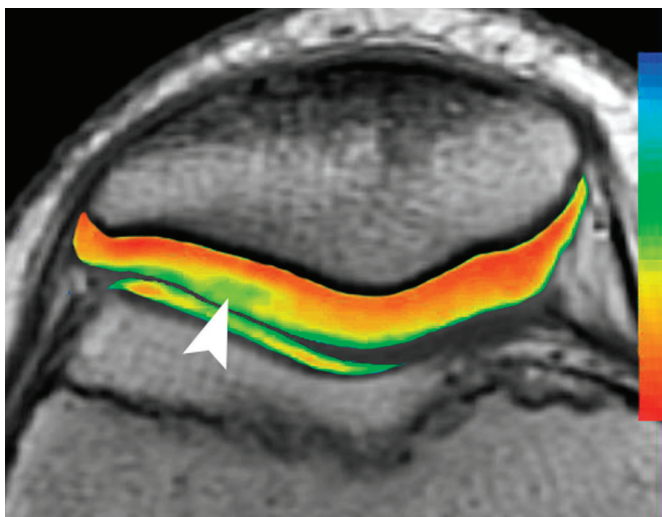

Fig. 7
Axial quantitative T2-relaxation-time map of the patellofemoral joint cartilage, color-coded to reflect T2 values ranging from 10 to 90 msec, with green/blue reflecting longer T2 values, yellow reflecting intermediate values, and orange/red reflecting shorter values. The normal medial facet demonstrates the expected stratification of T2 values, with the shortest values seen within the deep (radial) zone. Focal superficial prolongation of T2 relaxation times is noted in the lateral facet (arrowhead), indicating an alteration in the collagen component of the extracellular matrix.

imaging with or without fat saturation, or T1-weighted gradient-echo imaging for the evaluation of both native and repaired cartilage[9].

Classification

Many scoring systems have been described for the evaluation of articular cartilage[9-12]. The Outerbridge system is a well-known arthroscopic classification system that divides lesions into four grades but does not include a description of lesion depth for grade-II and III lesions[10]. Other systems have been described but are more appropriate for the evaluation of osteoarthritis and have not been widely used[12,13]. The ICRS, founded in 1997, developed a standardization system for the evaluation of cartilage injury and repair[9]. The ICRS arthroscopic scores have been validated for the assessment of cartilage repair and found to be statistically reliable and repeatable (Table I)[14].
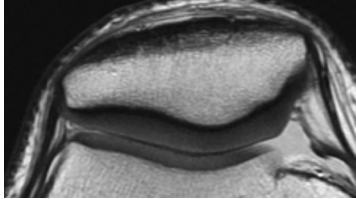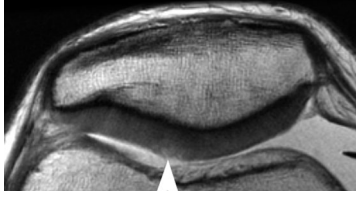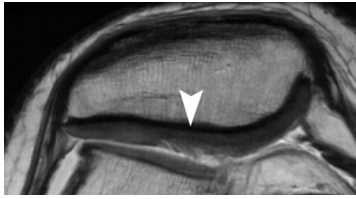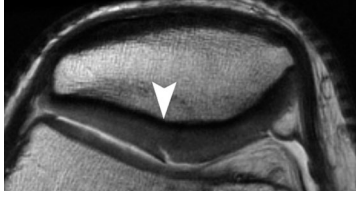
Novel Imaging Techniques

Novel approaches have been developed to supplement traditional magnetic resonance techniques for the assessment of cartilage morphology. Some of these techniques target different components of the extracellular matrix. For example, sodium magnetic resonance imaging[15], T1-weighted imaging with intravenous injection of negatively charged gadolinium-based compounds[16,17] and T1rho magnetic resonance imaging[18,19]

Fig. 8
Coronal fast-spin-echo magnetic resonance image of the knee in a thirty-year-old athlete with an acute complete anterior cruciate ligament tear, demonstrating a full-thickness cartilage defect over the lateral tibial plateau (black arrowhead). A complete proximal tear of the medial collateral ligament (white arrowhead) is also noted.

TABLE I Modified International Cartilage Repair Society Classification System			
Pathologic Change	Arthroscopic Findings	Magnetic Resonance Imaging Findings	Magnetic Resonance Images
Normal articular cartilage	Grade 0	Normal cartilage with gray-scale stratification	
Superficial lesions, chondral softening	Grade 1: softening to probe	Increased signal in articular cartilage	
Superficial lesions extending down to <50% of cartilage depth	Grade 2: fissures/fibrillation involving <50% thickness	Linear-to-ovoid foci of increased signal involving <50% thickness	Fibrillation < 50% Fissure < 50%
Cartilage defects extending down >50% of depth but not through subchondral bone	Grade 3: blisters/fissures/ fibrillation involving >50% thickness	Linear-to-ovoid foci of increased signal involving >50% of cartilage thickness but not extending down to bone	
Ulceration to subchondral bone	Grade 4: exposed subchondral bone	Complete loss of articular cartilage or surface flap	
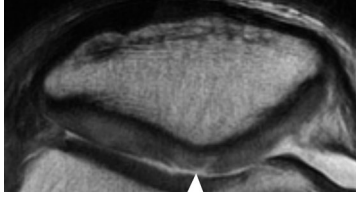
all target proteoglycans. T2 mapping, on the other hand, targets collagen orientation, and the T2 relaxation time is a function of the free water content of the tissue[20,21] (Fig. 7). In the deep zone, where the collagen is highly ordered and perpendicular to subchondral bone, T2 values are short because water is relatively immobilized. In the middle zone, where the collagen orientation is more random, water is more mobile and thus T2 values are relatively longer. The superficial zone is generally considered to be beyond the resolution of the current clinical field strengths[3].

Magnetic Resonance Imaging of Articular Cartilage of the Knee

Articular cartilage injuries in the knee are common[22], can clinically mimic meniscal tears[23,24], and have been associated with a less satisfactory clinical outcome following

Fig. 9

Sagittal fast-spin-echo magnetic resonance image of the knee, demonstrating articular cartilage delamination (arrowhead), with fluid signal intensity seen between the cartilage flap and the underlying subchondral bone.

arthroscopy[25]. Thus, magnetic resonance imaging prior to surgical intervention is valuable to evaluate for isolated articular cartilage injuries, to help to predict prognosis, and to identify patients who may benefit from cartilage replacement therapies[26].

Acute or repetitive trauma can cause a variety of articular cartilage injuries, including fissures, chondral flaps or tears, and loss of a segment of articular cartilage[27]. These injuries can occur in isolation[24] but usually are associated with other intra-articular injuries such as an acute anterior cruciate ligament tear[24,28] (Fig. 8). The knee may be exposed to various forces, including compression and shear forces, which can cause different forms of lesions to the articular cartilage and bone. Most osteochondral lesions are caused by shear forces, and osteochondritis dissecans may be the result of an ununited osteochondral fracture[29].

Cartilage Delamination

Chondral delamination is the separation of the articular cartilage from the underlying subchondral bone at the tidemark as the result of shear stresses. A linear signal abnormality will be present at the junction of the articular cartilage and the subchondral bone[30] (Fig. 9). These injuries, when left untreated or unrecognized, have been associated with a poor prognosis[31]. Impending delamination also can be detected with magnetic resonance imaging, which will demonstrate a hyperintense signal of the cartilage involving the radial (deep) layer without separation (Fig. 10).

Cartilage Shear Injury

Acute traumatic events can lead to chondral shear injuries and usually are associated with other intra-articular abnormalities such as meniscal tears (Figs. 11-A and 11-B). They often accompany complex joint injuries.

Osteochondral Fracture

Acute traumatic events also can lead to osteochondral fractures that may become displaced and can mimic a displaced meniscal tear. In the acute setting, bone marrow edema will be present (Figs. 12-A and 12-B). Eventually, the bone marrow edema will resolve and the underlying subchondral bone will remodel (Figs. 13-A and 13-B).

Transchondral Fracture

These injuries also occur as a result of acute traumatic events and usually are associated with other injuries, such as an acute anterior cruciate ligament tear (Figs. 14-A and 14-B).

Osteochondritis Dissecans

These injuries are due to separation or fragmentation of a portion of subchondral bone along the articular surface due to repetitive trauma or an acute shear injury. The most common site is the lateral aspect of the medial femoral condyle. Magnetic resonance imaging is important to assess for stability of the lesion, and signs of an unstable fragment include a size of >5 mm, high signal intensity surrounding the fragment on T2-weighed or short tau inversion-recovery images, cystic changes of ≥5 mm between the fragment and host bone, and a high-signal-intensity defect in the overlying cartilage[32] (Figs. 15-A through 15-D).

Fig. 10

Sagittal fast-spin-echo magnetic resonance image of the knee demonstrates high signal intensity of the cartilage involving the deep (radial) layer (arrowhead), indicating impending delamination.
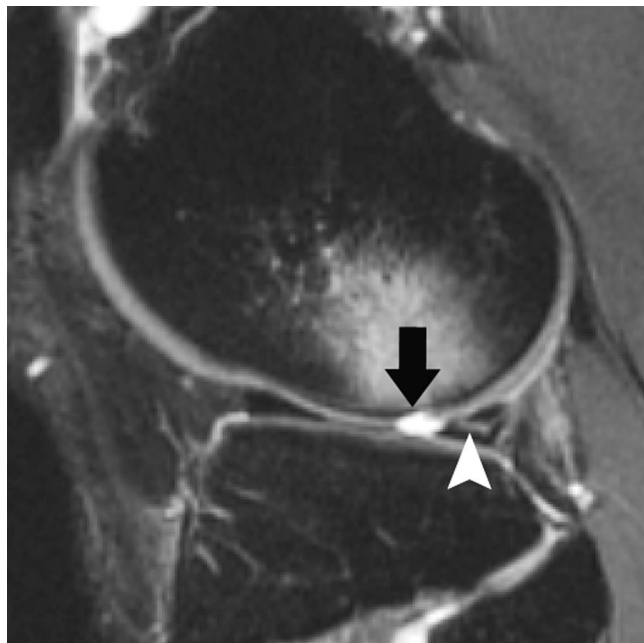
Fig. 11-A

Fig. 11-B

Sagittal fat-suppressed (Fig. 11-A) and non-fat-suppressed (Fig. 11-B) fast-spin-echo magnetic resonance images of the knee in a twenty-six-year-old professional football player with lateral joint-line tenderness following a knee injury. A clinically suspected lateral meniscal tear is confirmed (arrowheads), but an unsuspected chondral shear injury is also disclosed (arrows).

Magnetic Resonance Imaging of Articular Cartilage of the Hip

Because of the deep ball and socket configuration of the hip joint, articular cartilage injuries are difficult to evaluate. In addition, the articular cartilage is relatively thin. The curved articular surfaces of both the femoral head and the acetabulum should be evaluated with use of all three imaging planes. Some authors have advocated the use of magnetic resonance arthrography in

Fig. 12-A

Fig. 12-B

Sagittal fat-suppressed (Fig. 12-A) and coronal non-fat-suppressed (Fig. 12-B) fast-spin-echo magnetic resonance images of the knee in a fifteen-year-old cheerleader, following an acute traumatic patellar dislocation. A bone marrow edema pattern is present at the typical site of impaction over the anterolateral femoral condyle (white arrow). There is an associated osteochondral injury present (black arrow).

Fig. 13-A

Fig. 13-B

Sagittal fat-suppressed (Fig. 13-A) and non-fat-suppressed (Fig. 13-B) fast-spin-echo magnetic resonance images of the knee in a patient with a chronic osteochondral injury, demonstrating the absence of a bone marrow edema pattern. Remodeling of the underlying subchondral bone (arrows) results in proud bone anteriorly and depression posteriorly. Note the full-thickness cartilage defect.

order to improve contrast between the synovial fluid and cartilage[33-35]; however, this technique converts magnetic resonance imaging into a more invasive procedure. Mintz et al. evaluated ninety-two patients prior to hip arthroscopy and concluded that noncontrast imaging, with use of an optimized protocol, can identify labral and chondral abnormalities noninvasively[36].
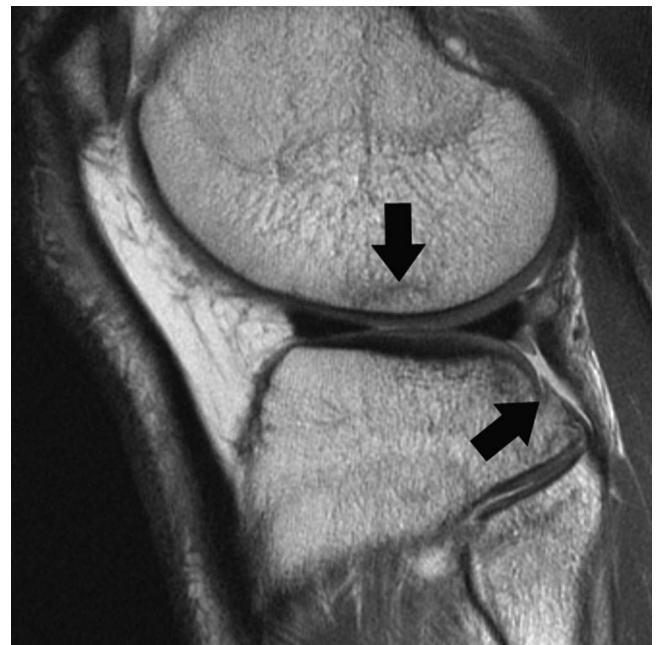

Fig. 14-A

Fig. 14-B

Sagittal fat-suppressed (Fig. 14-A) and non-fat-suppressed (Fig. 14-B) fast-spin-echo magnetic resonance images of the knee in a thirty-year-old skier with an acute, complete anterior cruciate ligament tear. Characteristic transchondral fractures (black arrows) and bone marrow edema pattern are present as a result of impaction of the lateral femoral condyle by the tibial plateau.

Magnetic Resonance Imaging of Cartilage in the Athlete:
Current Techniques and Spectrum of Disease

Femoroacetabular Impingement (Cam Lesion)
Femoroacetabular impingement is a pathologic condition characterized by a decreased osseous offset at the femoral head-neck junction (Figs. 16-A and 16-C) that is accentu-

ated on images obtained in the oblique axial plane (Fig. 16-B) (also known as the "Swiss protocol") along the axis of the femoral neck. Shear forces of the nonspherical portion of the femoral head against the acetabulum result in a characteris-
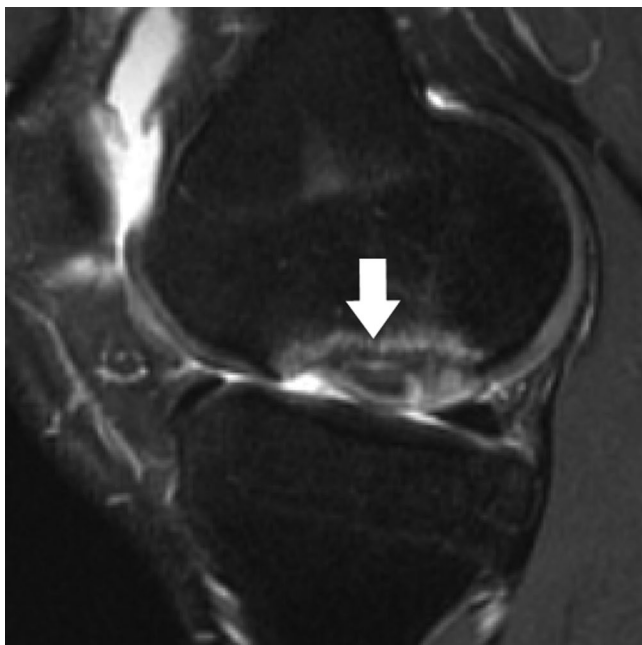

Fig. 15-A

Fig. 15-B

Fig. 15-C

Fig. 15-D

Figs. 15-A through 15-D Sagittal fat-suppressed (Fig. 15-A) and coronal non-fat-suppressed (Fig. 15-B) fast-spin-echo magnetic resonance images of the knee in a thirteen-year-old patient with a small, stable osteochondritis dissecans lesion (arrowheads). In comparison, magnetic resonance images in a twenty-three-year-old patient (Figs. 15-C and 15-D) demonstrate a larger, unstable lesion (arrows), with low-signal-intensity sclerosis at the margins of the underlying bone, indicating the presence of a "mature" bed. In addition, the lesion has been partially delaminated from its site of origin.

tic pattern of cartilage loss over the anterosuperior weight-bearing portion of the dome (Fig. 16-D). Although focal separation between the labrum and the articular cartilage may occur, the labrum itself often remains untouched[37].

Magnetic resonance imaging is also useful for preoperative planning to determine the site of bone resection (Figs. 16-A and 16-C), to assess the integrity of the cartilage, and to detect additional labral lesions.
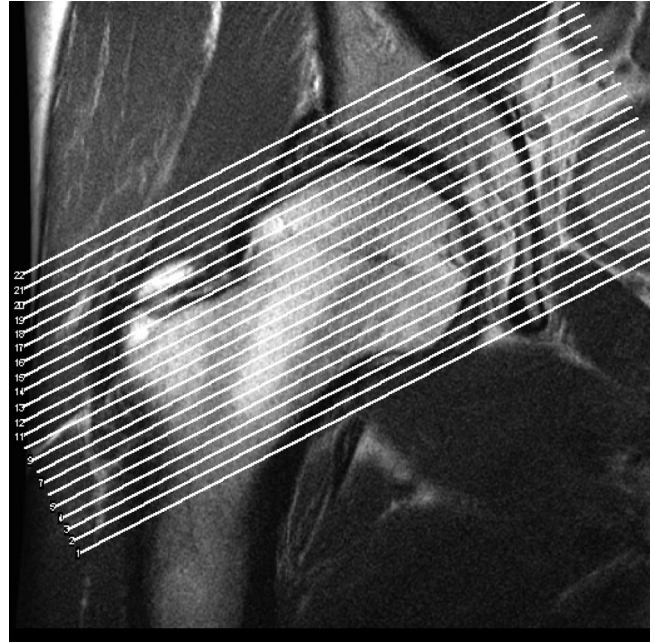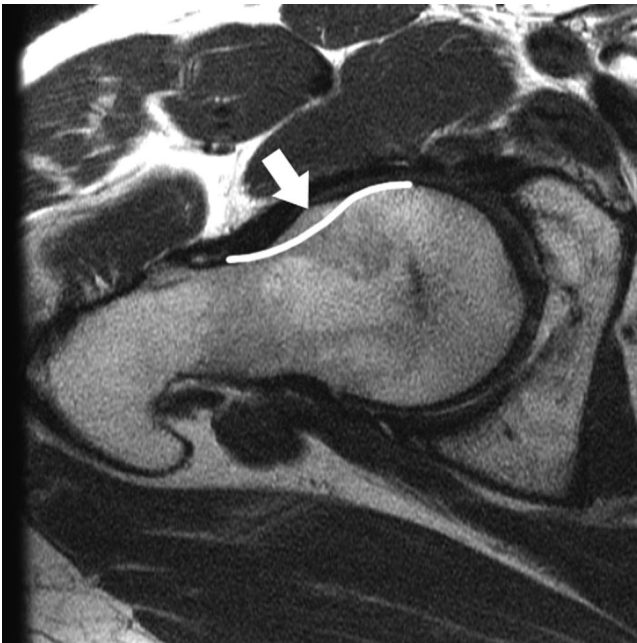

Fig. 16-A

Fig. 16-B

Fig. 16-C

Fig. 16-D

Figs. 16-A through 16-D Fast-spin-echo magnetic resonance images of a forty-one-year-old patient with cam-type femoral acetabular impingement. The coronal image (Fig. 16-A) demonstrates osseous offset at the neck-shaft junction (white arrow) and ossification of a torn superior labrum (white arrowhead). Slice prescription (Fig. 16-B) of the oblique axial view (Fig. 16-C) of the right hip accentuates the osseous offset. The sagittal image (Fig. 16-D) demonstrates full-thickness cartilage loss over the anterior acetabular dome (black arrow) and partial thickness of the anterior femoral head. These images can aid in preoperative planning to determine the site of bone resection (see curved lines in Figs. 16-A and 16-C).

Fig. 17-A

Fig. 17-B

Sagittal (Fig. 17-A) and coronal (Fig. 17-B) fast-spin-echo magnetic resonance images of the hip in a twenty-eight-year-old patient with pincer-type femoroacetabular impingement. A chronically degenerated and torn anterosuperior labrum (arrows) is seen.

Femoroacetabular Impingement (Pincer Lesion)

Repetitive contact stresses of a normal femoral neck against an abnormal anterior acetabular rim as a result of "overcoverage" or retroversion result in degeneration, ossification, and tears of the anterosuperior labrum (Figs. 17-A and 17-B) as well as a characteristic posteroinferior "contre-coup" pattern of cartilage loss over the femoral head and corresponding acetabulum. In pure pincer lesions, the acetabular cartilage is characteristically preserved.

Combined Impingement

The majority of cases of femoroacetabular impingement involve a combination of femoral side and acetabular side lesions. Beck et al. found that 86% of investigated cases had combined lesions, where only 9% had isolated femoral side impingement and 5% had isolated acetabular side impingement[37]. Careful evaluation of the magnetic resonance image preoperatively will provide important data regarding the underlying pathology and guidance for treatment options[38-41].

Posterior Hip Dislocation/Subluxation

In both of these injuries, magnetic resonance imaging helps to identify the presence of chondral shear injuries of the femoral head and to evaluate for large cartilaginous loose bodies in the central and peripheral compartments (Figs. 18-A, 18-B, and 18-C). In a study of patients with posterior hip subluxations, Moorman et al. described the pathognomonic magnetic resonance imaging triad of posterior acetabular lip fracture, iliofemoral ligament disruption, and hemarthrosis[42]. The presence of a notable hemarthrosis may warrant aspiration with use of fluoroscopy to decrease intracapsular pressure. In addition, magnetic resonance imaging is also a useful tool for the detection of subsequent osteonecrosis that can result in a delay of return to play[42].

Magnetic Resonance Imaging of Articular Cartilage in Smaller Joints

Due to the thinner cartilage in the shoulder, elbow, and ankle, detecting articular cartilage lesions is challenging and requires a superior surface coil design and imaging technique.

Shoulder

Although less common than those of the lower extremity, articular cartilage lesions of the shoulder do occur and can cause severe symptoms including pain, effusions, and mechanical dysfunction[43-46]. Magnetic resonance imaging of the shoulder is useful for identifying these lesions and also for detecting abnormalities that may mimic or occur in conjunction with rotator cuff (Fig. 19) or labral (Figs. 20-A and 20-B) abnormalities[47].

Ankle/Foot

Magnetic resonance imaging of the ankle may be performed to evaluate for chondral or osteochondral shear injuries[48].

Osteochondral Injuries

Magnetic resonance imaging is useful to evaluate the extent of the lesion and the stability of the fragment[32]. Osteochondral injuries of the talar dome can affect both the medial and lateral aspects of the dome (Fig. 21) and occur most commonly in the second to fourth decades of life[48]. Al-

though relatively uncommon, the majority of these injuries are undiagnosed. Takao et al. demonstrated that 71% of patients with ankle fractures and 41% of patients with chronic lateral instability had evidence of an osteochondral lesion on the basis of an arthroscopic or magnetic resonance imaging evaluation[49].

Chondral Shear Injury
As in the knee, these injuries usually are caused by an acute traumatic event (Fig. 22).

Turf Toe
Magnetic resonance imaging will demonstrate disruption of

Fig. 18-A

Fig. 18-B

Fig. 18-C

Figs. 18-A, 18-B, and 18-C Axial body coil (Fig. 18-A) as well as sagittal surface coil (Figs. 18-B and 18-C) fast-spin-echo magnetic resonance images of the hip in an eighteen-year-old patient with sequelae of posterior hip subluxation. An intact posterior hip capsule is seen, attached to a posterior wall fracture (Fig. 18-A, white arrowhead). A large full-thickness chondral shear injury (Fig. 18-B, black arrow) of the femoral head is well depicted. Cartilaginous debris (Fig. 18-C, white arrow) is seen within the anteroinferior dependent recess of the joint.

Fig. 19

Coronal oblique fast-spin-echo magnetic resonance image of the shoulder in a patient with supraspinatus tendinosis, demonstrating full-thickness cartilage loss over the humeral head (arrow) with flap formation. Debris in the axillary pouch (arrowhead) and a joint effusion are also noted.

the plantar plate and capsule but is also useful for identifying associated chondral lesions (Fig. 23) that may result in delayed recovery because of stiffness.
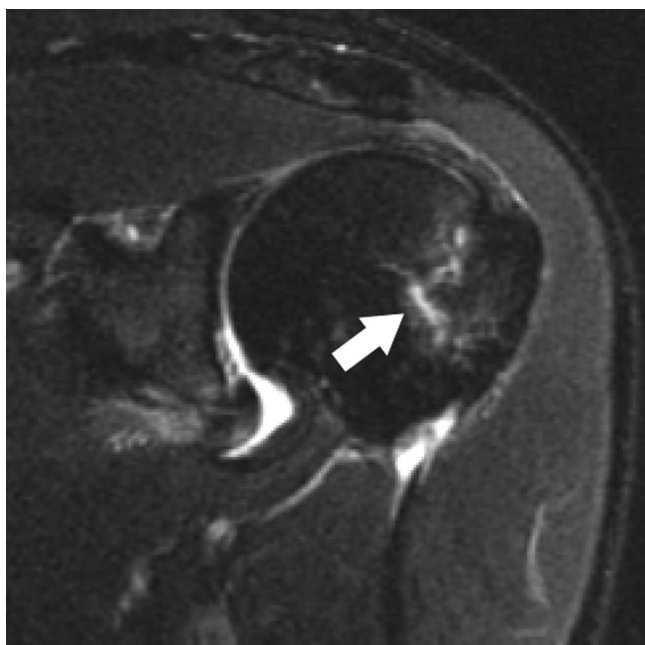
Elbow
Throwing athletes are particularly vulnerable to valgus stress injuries of the elbow. The large valgus moment across the elbow causes compression at the radiocapitellar joint[50]. Thus, osteochondral or chondral injuries of the capitellum (Fig. 24) or trochlea may develop and lead to mechanical symptoms with activity and lateral elbow pain[5].

Posteromedial Impingement
Impingement may occur in high-level athletes because of the olecranon repeatedly striking against the posterior part of the humerus, resulting in a characteristic posteromedial osteophyte and chondral wear off the posterior margin of the trochlea (Figs. 25-A and 25-B).

Magnetic Resonance Imaging of Articular Cartilage Repair Techniques

Articular cartilage injuries remain a common and challenging problem. Mature articular cartilage has limited reparative capacity because of its limited vascular supply. A number of techniques have been described for the repair of articular injuries; however, the results and clinical outcomes have varied widely. Most of the literature has relied on the use of second-look surgery along with biopsy to evaluate the results of articular cartilage repair. With the advances in imaging techniques and sequence development, magnetic resonance imaging offers an alternative method of noninvasively evaluating the results of articular cartilage repair procedures.

According to Brown et al., a number of variables should be assessed when evaluating the quality of articular cartilage fol-

Fig. 20-A

Fig. 20-B

Coronal oblique fat-suppressed (Fig. 20-A) and non-fat-suppressed (Fig. 20-B) fast-spin-echo magnetic resonance images of the shoulder in a patient following an acute traumatic anterior shoulder dislocation. An anteroinferior labral tear (Bankart lesion) and an adjacent full-thickness cartilage defect of the glenoid (arrowhead) are seen. Recent impaction is also noted (arrow).
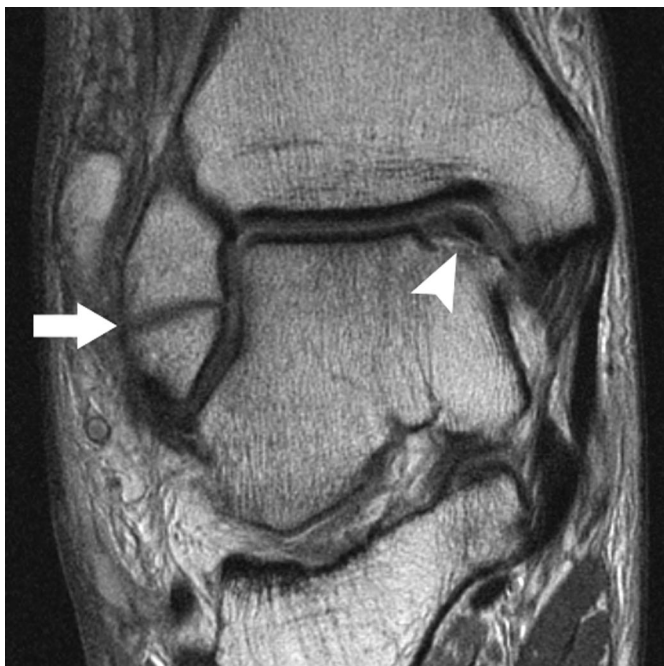
Fig. 21

Coronal fast-spin-echo magnetic resonance image of the ankle in a patient with a distal fibular fracture (arrow) following an injury. An associated osteochondral injury (arrowhead) of the anteromedial talar dome is also present, with loss of continuity of the subchondral bone and overlying cartilage. No features of instability are demonstrated.

Fig. 22

Coronal fast-spin-echo magnetic resonance image of the ankle in a patient with an avulsion fracture of the fibular tip following an inversion injury, demonstrating an unsuspected concomitant full-thickness chondral shear injury with flap formation (arrowhead) over the medial talar dome.

Fig. 23

Sagittal fast-spin-echo magnetic resonance image of an elite athlete with clinically suspected turf toe, demonstrating disruption of the plantar plate (white arrowhead) as well as full-thickness cartilage loss over the first metatarsal head (black arrowhead).

Fig. 24

Sagittal fast-spin-echo magnetic resonance image of the elbow in a professional baseball player, demonstrating a partial-thickness cartilage injury over the capitellum (arrow).
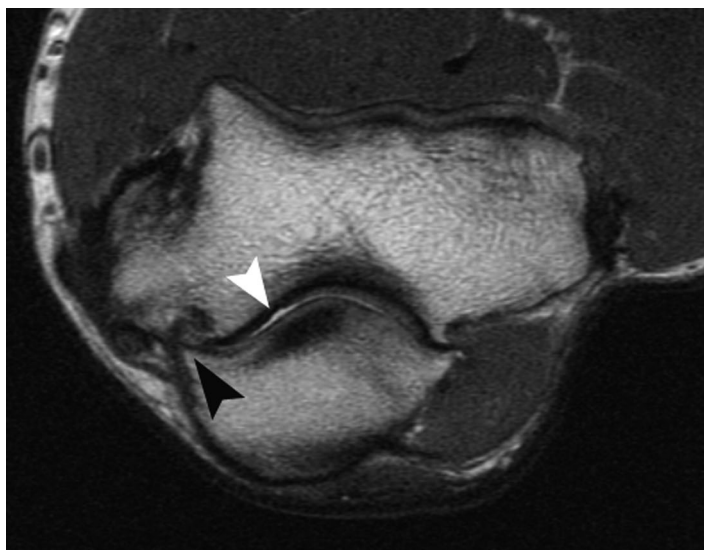
Fig. 25-A

Figs. 25-A and 25-B Axial (Fig. 25-A) and sagittal (Fig. 25-B) fast-spin-echo magnetic resonance images of the elbow in a professional baseball pitcher with valgus extension overload. There is an osteophyte extending off the posteromedial margin of the olecranon (black arrowhead), full-thickness cartilage loss in the posteromedial margin of the trochlea (white arrowhead), sclerosis of the olecranon, and dense scarring of the posterosuperior capsule (white arrow).

Fig. 25-B

lowing repair[51]. These variables include the relative signal intensity of the regenerated cartilage as compared with the surrounding native tissue, the surface geometry and morphology of the repaired tissue, the presence or absence of displacement, the degree of peripheral integration to adjacent cartilage and/or underlying bone, the degree of defect filling, and the presence of any reactive synovitis[51].

Microfracture is a cartilage repair technique that is based on local bone marrow stimulation and is readily performed arthroscopically. This procedure relies on the release of multipotential stem cells from the bone marrow underlying a cartilage defect. The cells are released by creating perforations in the underlying subchondral bone with use of a drill or pick. The bleeding bone then forms a clot containing the multipotential stem cells. Over time, the cells differentiate and form a tissue that consists primarily of fibrocartilage. This reparative tissue is less organized, with increased water content as compared with native cartilage[52]. As such, reparative tissue from microfracture will tend to be hyperintense as compared with native cartilage (Figs. 26-A and 26-B). Overgrowth of the underlying subchondral bone has been noted in other studies[53]. This of itself does not appear to be a negative prognostic factor[54]. However, osseous overgrowth may result in a thinner layer of reparative tissue with inferior defect filling, which has been found to correlate with inferior functional outcomes[54].

Autologous chondrocyte implantation is a technique whereby a patient's native chondrocytes are harvested arthro-

scopically and subsequently are grown in tissue culture for a period of three to five weeks. During subsequent surgery, which requires an open arthrotomy, periosteum harvested from the patient is sewn over the cartilage defect with the cambium layer facing the defect. The edges are then secured with sutures and/or fibrin glue. The previously cultured chondrocytes are then injected under this periosteal cover. The appearance of reparative tissue following autologous chondrocyte implantation varies with time. Initially, the reparative tissue remains disorganized with increased water content; consequently, it appears hyperintense on magnetic resonance images[55] (Fig. 27-A). This hyperintensity contrasts markedly with the overlying periosteum, which appears hypointense, allowing the two structures to be readily differentiated. Once fully incorporated, however, the periosteal cover remains undistinguishable. Three to six months after repair, other authors have observed a decline in the signal intensity of the reparative tissue as it becomes increasingly organized and integrated with the surrounding tissue (Fig. 27-B). While uncommon, delamination of the reparative tissue due to incomplete integration can be a notable problem[56]. This most commonly occurs within the first six months after surgery and is seen as a hyperintense fluid signal between the reparative tissue and the underlying bone[57,58]. Complete integration has been found to take up to two years. While autologous chondrocyte implantation has been found to provide better defect fill as compared with microfracture, overgrowth of the reparative tissue has

Magnetic Resonance Imaging of Cartilage in the Athlete:
Current Techniques and Spectrum of Disease

been problematic with autologous chondrocyte implantation, largely because of hypertrophy of the periosteum at early follow-up intervals[51].

The use of autologous osteochondral plugs involves the harvest of osteochondral plugs from a non-weight-bearing portion of the knee in the same individual. Common sites for obtaining the plugs include the anterior margin of the femoral condyle and the side of the intercondylar notch. Osteochondral

Fig. 26-A

Fig. 26-B

Figs. 26-A and 26-B Sagittal fast-spin-echo magnetic resonance images of the knee in a thirty-two-year-old patient following microfracture. At five months of follow-up (Fig. 26-A) there is irregularity of the subchondral plate (white arrow) adjacent to the hyperintense repair cartilage. A corresponding image at thirteen months of follow-up (Fig. 26-B) demonstrates mature repair cartilage that is now partially hypointense (black arrow) compared with the adjacent cartilage. Note also the presence of subtle overgrowth of subchondral bone.

Fig. 27-A

Fig. 27-B

Figs. 27-A and 27-B Coronal fast-spin-echo magnetic resonance images of the knee in a fifteen-year-old patient, made eight months after autologous chondrocyte implantation (Fig. 27-A) for the treatment of osteochondritis dissecans, demonstrating increased signal intensity of the graft (arrowhead). At twenty-seven months of follow-up (Fig. 27-B), there is "maturation" of the repair cartilage, which is now approaching that of the adjacent native cartilage (arrow), but with interval thinning at the notch.

plugs of varying shapes and sizes can be harvested and transferred in varying combinations to fill the defect of interest. There are several characteristics unique to autologous osteochondral transplants that can be assessed with use of magnetic resonance imaging, including the integration of the osseous portion of the plug as well as the accuracy of restoring the surface morphology and radius of curvature (Figs. 28-A and 28-B). The osseous portion of the plug typically demonstrates excellent incorporation; however, persistent gaps at the cartilaginous level between the graft and the native tissue (Fig. 28-D) have been found in several studies[58]. The appearance of a hypointense signal at the osseous interface is indicative of adjacent sclerosis due to the tight fit created in the commonly used "press-fit" technique (Fig. 28-C). Any failure of integration of the osseous plug would appear as a hyperintense signal at the native bone-graft interface[57].

Osteochondral allograft plugs are most commonly utilized for the treatment of intermediate to large-sized lesions in physically active patients. This procedure involves the use of an
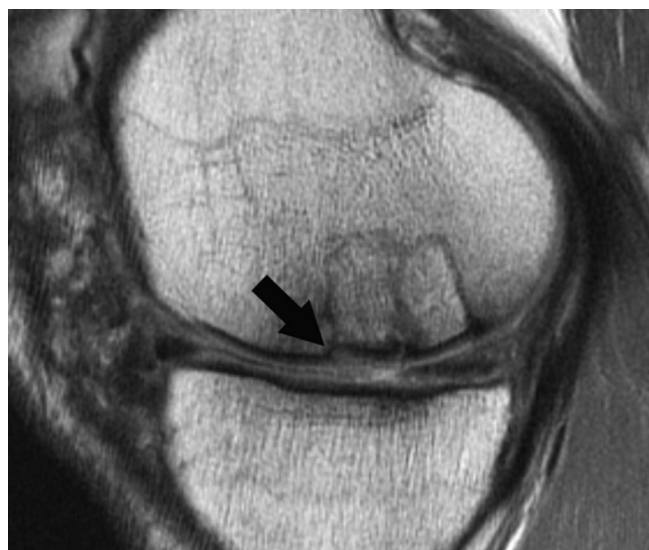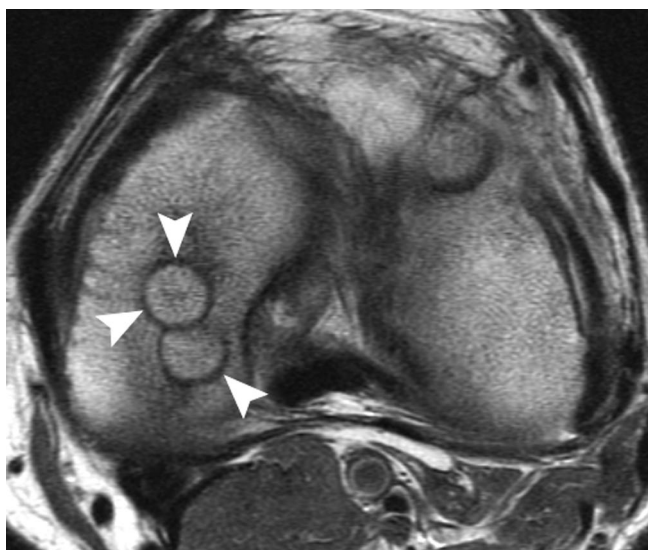

Fig. 28-A

Fig. 28-B

Fig. 28-C

Fig. 28-D

Figs. 28-A through 28-D Magnetic resonance images of the knee in a fifty-two-year-old patient, made after the transfer of two autologous osteochondral plugs. Sagittal fat-suppressed (Fig. 28-A) and non-fat-suppressed (Fig. 28-B) fast-spin-echo images demonstrate osseous incorporation of the plugs. Note the slight sclerosis in the side wall of the plugs in the axial plane (white arrowheads, Fig. 28-C), reflecting the "press-fit" technique. Although there is slight depression of the subchondral bone over the anterior plug (Fig. 28-B, black arrow), the cartilage surface remains flush. A fissure at the lateral interface with the native cartilage is seen on the coronal magnetic resonance image (Fig. 28-D, white arrow). There is a degenerative pattern of partial-thickness cartilage loss over the medial tibial plateau.
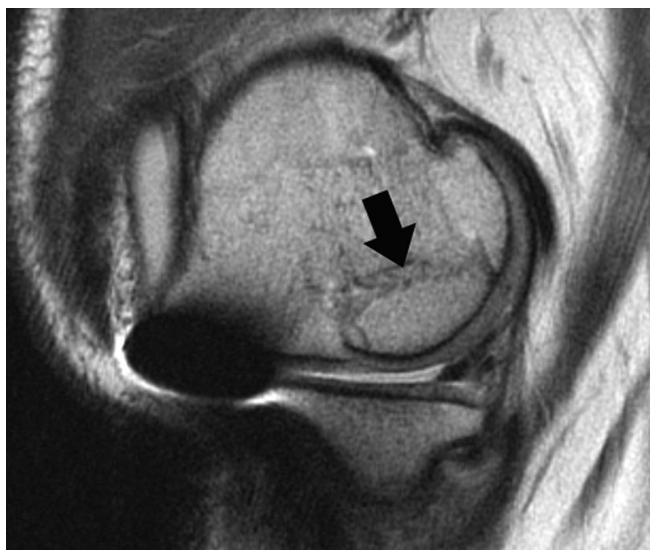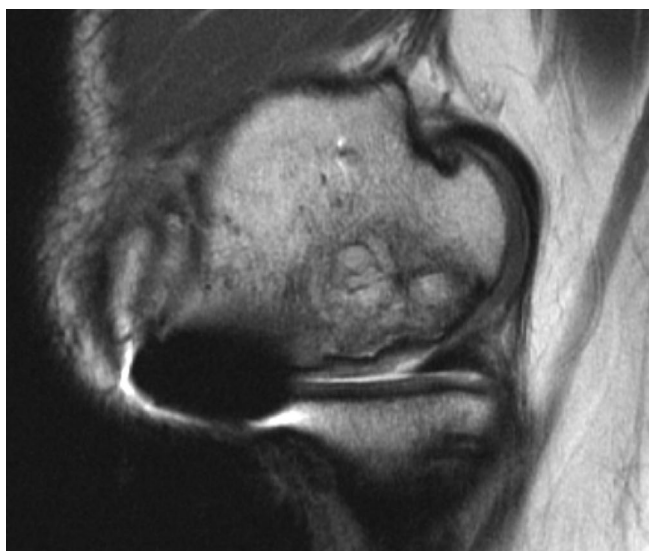
Fig. 29-A

Fig. 29-B

Fig. 29-C

Figs. 29-A, 29-B, and 29-C Sagittal fast-spin-echo magnetic resonance images of the knee in a forty-six-year-old patient with progressive collapse of an allograft osteochondral transfer. At the time of early follow-up (Fig. 29-A), incomplete osseous incorporation (black arrow) of the graft is seen. At nine months of follow-up (Fig. 29-B), there is sclerosis of bone at the graft-host bone interface (white arrow). The low-signal-intensity subchondral bone (white arrowhead) indicates devitalized bone with partial collapse. This subsequently led to graft failure (Fig. 29-C).

osteochondral plug harvested from a cadaver and is not indicated for superficial or small lesions because it creates a subchondral defect. Osteochondral allograft plugs usually are placed with use of a "press-fit" technique whereby the plug and the recipient site are prepared to matching sizes. In some cases, particularly for larger plugs, supplemental fixation, such as with use of biodegradable pins, may be required to ensure stable fixation between the donor tissue and the native tissue. As with autologous plugs, the degree of osseous integration and the restoration of the surface architecture are unique and important characteristics to assess on magnetic resonance images (Figs. 29-A and 29-B). Persistent clefts in the articular surface also are a problem with allograft plugs. As the donor tissue is obtained from a foreign host, there is the potential for an immunologic reaction, typically characterized by a persistent, hyperintense signal on magnetic resonance images[58]. Furthermore, grafts that

Fig. 30

Coronal fast-spin-echo magnetic resonance image of the knee in a patient following implantation of a synthetic scaffold bone-graft substitute. Note that the signal characteristics are distinctly different from those of autologous or cadaveric bone. The implant is flush with adjacent native articular surface.

fail to demonstrate notable osseous integration often result in subchondral collapse (Fig. 29-C).

Synthetic bone-graft-substitute implants are now available for use, obviating the need for autologous or allograft tissue harvesting, with distinctly different appearances on magnetic resonance imaging (Fig. 30).

Conclusion

Magnetic resonance imaging is playing an increasing role in the noninvasive diagnosis of articular cartilage lesions and for the objective assessment of chondral repair techniques, providing important information to augment that obtained from more subjective standardized clinical outcome instruments. With continued pulse sequence refinement, additional early detection of changes in the extracellular matrix elements will become more available. ∎

Corresponding author:
Hollis G. Potter, MD
Department of Radiology and Imaging, MRI Division, Hospital for Special Surgery, 535 East 70th Street, New York, NY 10021. E-mail address: potterh@hss.edu

References

1. West RV, Fu FH. Soft-tissue physiology and repair. In: Vaccaro AR, editor. Orthopaedic knowledge update 8. Home study syllabus. Rosemont, IL: American Academy of Orthopaedic Surgeons; 2005. p 15-28.

2. Mow VC, Proctor CS, Kelly MA. Biomechanics of articular cartilage. In: Nordin M, Frankel VH, editors. Basic biomechanics of the musculoskeletal system. Philadelphia: Lea and Febiger; 1989. p 31-57.

3. Potter HG, Foo LF. Magnetic resonance imaging of articular cartilage: trauma, degeneration, and repair. Am J Sports Med. 2006;34:661-77.

4. Potter HG, Linklater JM, Allen AA, Hannafin JA, Haas SB. Magnetic resonance imaging of articular cartilage in the knee. An evaluation with use of fast-spin-echo imaging. J Bone Joint Surg Am. 1998;80:1276-84.

5. Manaster BJ, Johnson T, Narahari U. Imaging of cartilage in the athlete. Clin Sports Med. 2005;24:13-37.

6. Kassarjian A, Yoon LS, Belzile E, Connolly SA, Millis MB, Palmer WE. Triad of MR arthrographic findings in patients with cam-type femoroacetabular impingement. Radiology. 2005;236:588-92.

7. Kramer J, Recht MP. MR arthrography of the lower extremity. Radiol Clin North Am. 2002;40:1121-32.

8. Schmid MR, Notzli HP, Zanetti M, Wyss TF, Hodler J. Cartilage lesions in the hip: diagnostic effectiveness of MR arthrography. Radiology. 2003;226:382-6.

9. Brittberg M, Winalski CS. Evaluation of cartilage injuries and repair. J Bone Joint Surg Am. 2003;85:58-69.

10. Outerbridge RE. The etiology of chondromalacia patellae. 1961. Clin Orthop Relat Res. 2001;389:5-8.

11. Dougados M, Ayral X, Listrat V, Gueguen A, Bahuaud J, Beaufils P, Beguin JA, Bonvarlet JP, Boyer T, Coudane H, Delaunay C, Dorfmann H, Dubos JP, Frank A, Kempf JF, Locker B, Prudhon JL, Thiery J. The SFA system for assessing articular cartilage lesions at arthroscopy of the knee. Arthroscopy. 1994;10:69-77.

12. Noyes FR, Stabler CL. A system for grading articular cartilage lesions at arthroscopy. Am J Sports Med. 1989;17:505-13.

13. Ayral X, Dougados M, Listrat V, Bonvarlet JP, Simonnet J, Poiraudeau S, Amor B. Chondroscopy: a new method for scoring chondropathy. Semin Arthritis Rheum. 1993;22:289-97.

14. Smith GD, Taylor J, Almqvist KF, Erggelet C, Knutsen G, Garcia Portabella M, Smith T, Richardson JB. Arthroscopic assessment of cartilage repair: a validation study of 2 scoring systems. Arthroscopy. 2005;21:1462-7.

15. Reddy R, Insko EK, Noyszewski EA, Dandora R, Kneeland JB, Leigh JS. Sodium MRI of human articular cartilage in vivo. Magn Reson Med. 1998;39:697-701.

16. Bashir A, Gray ML, Boutin RD, Burstein D. Glycosaminoglycan in articular cartilage: in vivo assessment with delayed Gd(DTPA)(2-)-enhanced MR imaging. Radiology. 1997;205:551-8.

17. Williams A, Gillis A, McKenzie C, Po B, Sharma L, Micheli L, McKeon B, Burstein D. Glycosaminoglycan distribution in cartilage as determined by delayed gadolinium-enhanced MRI of cartilage (dGEMRIC): potential clinical applications. AJR Am J Roentgenol. 2004;182:167-72.

18. Wheaton AJ, Dodge GR, Elliott DM, Nicoll SB, Reddy R. Quantification of cartilage biomechanical and biochemical properties via T1rho magnetic resonance imaging. Magn Reson Med. 2005;54:1087-93.

19. Duvvuri U, Charagundla SR, Kudchodkar SB, Kaufman JH, Kneeland JB, Rizi R, Leigh JS, Reddy R. Human knee: in vivo T1(rho)-weighted MR imaging at 1.5 T—preliminary experience. Radiology. 2001;220:822-6.

20. Xia Y, Farquhar T, Burton-Wurster N, Ray E, Jelinski LW. Diffusion and relaxation mapping of cartilage-bone plugs and excised disks using microscopic magnetic resonance imaging. Magn Reson Med. 1994;31:273-82.

21. David-Vaudey E, Ghosh S, Ries M, Majumdar S. T2 relaxation time measurements in osteoarthritis. Magn Reson Imaging. 2004;22:673-82.

22. Curl WW, Krome J, Gordon ES, Rushing J, Smith BP, Poehling GG. Cartilage injuries: a review of 31,516 knee arthroscopies. Arthroscopy. 1997;13:456-60.

23. Disler DG, McCauley TR, Kelman CG, Fuchs MD, Ratner LM, Wirth CR, Hospodar PP. Fat-suppressed three-dimensional spoiled gradient-echo MR imaging of hyaline cartilage defects in the knee: comparison with standard MR imaging and arthroscopy. AJR Am J Roentgenol. 1996;167:127-32.

24. Terry GC, Flandry F, Van Manen JW, Norwood LA. Isolated chondral fractures of the knee. Clin Orthop Relat Res. 1988;234:170-7.

25. Northmore-Ball MD, Dandy DJ. Long-term results of arthroscopic partial meniscectomy. Clin Orthop Relat Res. 1982;167:34-42.

26. McCauley TR, Disler DG. Magnetic resonance imaging of articular cartilage of the knee. J Am Acad Orthop Surg. 2001;9:2-8.

27. Buckwalter JA. Articular cartilage injuries. Clin Orthop Relat Res. 2002; 402:21-37.

28. Indelicato PA, Bittar ES. A perspective of lesions associated with ACL insufficiency of the knee. A review of 100 cases. Clin Orthop Relat Res. 1985;198:77-80.

29. Tomatsu T, Imai N, Takeuchi N, Takahashi K, Kimura N. Experimentally produced fractures of articular cartilage and bone. The effects of shear forces on the pig knee. J Bone Joint Surg Br. 1992;74:457-62.

30. Kendell SD, Helms CA, Rampton JW, Garrett WE, Higgins LD. MRI appearance of chondral delamination injuries of the knee. AJR Am J Roentgenol. 2005;184:1486-9.

31. Levy AS, Lohnes J, Sculley S, LeCroy M, Garrett W. Chondral delamination of the knee in soccer players. Am J Sports Med. 1996;24:634-9.

32. De Smet AA, Ilahi OA, Graf BK. Reassessment of the MR criteria for stability of osteochondritis dissecans in the knee and ankle. Skeletal Radiol. 1996; 25:159-63.

33. Chan YS, Lien LC, Hsu HL, Wan YL, Lee MS, Hsu KY, Shih CH. Evaluating hip labral tears using magnetic resonance arthrography: a prospective study comparing hip arthroscopy and magnetic resonance arthrography diagnosis. Arthroscopy. 2005;21:1250.

34. Werlen S, Leunig M, Ganz R. Magnetic resonance arthrography of the hip in femoroacetabular impingement: technique and findings. Oper Tech Orthop. 2005;15:191-203.

35. Leunig M, Werlen S, Ungersbock A, Ito K, Ganz R. Evaluation of the acetabular labrum by MR arthrography. J Bone Joint Surg Br. 1997;79:230-4.

36. Mintz DN, Hooper T, Connell D, Buly R, Padgett DE, Potter HG. Magnetic resonance imaging of the hip: detection of labral and chondral abnormalities using noncontrast imaging. Arthroscopy. 2005;21:385-93.

37. Beck M, Kalhor M, Leunig M, Ganz R. Hip morphology influences the pattern of damage to the acetabular cartilage: femoroacetabular impingement as a cause of early osteoarthritis of the hip. J Bone Joint Surg Br. 2005;87:1012-8.

38. Chatha DS, Arora R. MR imaging of the normal hip. Magn Reson Imaging Clin N Am. 2005;13:605-15.

39. Bencardino JT, Palmer WE. Imaging of hip disorders in athletes. Radiol Clin North Am. 2002;40:267-87, vi-vii.

40. Meislin R, Abeles A. Role of hip MR imaging in the management of sports-related injuries. Magn Reson Imaging Clin N Am. 2005;13:635-40.

41. Bredella MA, Stoller DW. MR imaging of femoroacetabular impingement. Magn Reson Imaging Clin N Am. 2005;13:653-64.

42. Moorman CT 3rd, Warren RF, Hershman EB, Crowe JF, Potter HG, Barnes R, O'Brien SJ, Guettler JH. Traumatic posterior hip subluxation in American football. J Bone Joint Surg Am. 2003;85:1190-6.

43. Anderson WJ, Guilford WB. Osteochondritis dissecans of the humeral head. An unusual cause of shoulder pain. Clin Orthop Relat Res. 1983;173:166-8.

44. Scheibel M, Bartl C, Magosch P, Lichtenberg S, Habermeyer P. Osteochondral autologous transplantation for the treatment of full-thickness articular cartilage defects of the shoulder. J Bone Joint Surg Br. 2004;86:991-7.

45. Johnson DL, Warner JJ. Osteochondritis dissecans of the humeral head: treatment with a matched osteochondral allograft. J Shoulder Elbow Surg. 1997;6:160-3.

46. Ishikawa H, Ueba Y, Yonezawa T, Kurosaka M, Ohno O, Hirohata K. Osteochondritis dissecans of the shoulder in a tennis player. Am J Sports Med. 1988;16:547-50.

47. McCarty LP 3rd, Cole BJ. Nonarthroplasty treatment of glenohumeral cartilage lesions. Arthroscopy. 2005;21:1131-42.

48. Recht MP, Donley BG. Magnetic resonance imaging of the foot and ankle. J Am Acad Orthop Surg. 2001;9:187-99.

49. Takao M, Ochi M, Uchio Y, Naito K, Kono T, Oae K. Osteochondral lesions of the talar dome associated with trauma. Arthroscopy. 2003;19:1061-7.

50. Labbé MR, Savoie FH. Overuse elbow injuries. In: Garrick JG, editor. Orthopaedic knowledge update 3. Sports medicine. Rosemont, IL: American Academy of Orthopaedic Surgeons; 2004. p 91-100.

51. Brown WE, Potter HG, Marx RG, Wickiewicz TL, Warren RF. Magnetic resonance imaging appearance of cartilage repair in the knee. Clin Orthop Relat Res. 2004;422:214-23.

52. Mithoefer K, Williams RJ 3rd, Warren RF, Potter HG, Spock CR, Jones EC, Wickiewicz TL, Marx RG. The microfracture technique for the treatment of articular cartilage lesions in the knee. A prospective cohort study. J Bone Joint Surg Am. 2005;87:1911-20.

53. Verstraete KL, Almqvist F, Verdonk P, Vanderschueren G, Huysse W, Verdonk R, Verbrugge G. Magnetic resonance imaging of cartilage and cartilage repair. Clin Radiol. 2004;59:674-89.

54. Peterson L, Minas T, Brittberg M, Nilsson A, Sjogren-Jansson E, Lindahl A. Two- to 9-year outcome after autologous chondrocyte transplantation of the knee. Clin Orthop Relat Res. 2000;374:212-34.

55. Alparslan L, Minas T, Winalski CS. Magnetic resonance imaging of autologous chondrocyte implantation. Semin Ultrasound CT MR. 2001;22:341-51.

56. Alparslan L, Winalski CS, Boutin RD, Minas T. Postoperative magnetic resonance imaging of articular cartilage repair. Semin Musculoskelet Radiol. 2001;5:345-63.

57. Glenn RE Jr, McCarty EC, Potter HG, Juliao SF, Gordon JD, Spindler KP. Comparison of fresh osteochondral autografts and allografts: a canine model. Am J Sports Med. 2006;34:1084-93.

58. Sirlin CB, Brossmann J, Boutin RD, Pathria MN, Convery FR, Bugbee W, Deutsch R, Lebeck LK, Resnick D. Shell osteochondral allografts of the knee: comparison of MR imaging findings and immunologic responses. Radiology. 2001;219:35-43.